Downloaded by Fang Hu on August 28, 2016 | http://arc.aiaa.org | DOI: 10.2514/6.1999-3308



A99-33574

AIAA 99-3308 Application of Discontinuous Galerkin Method to Computational Acoustics

Fang Q. Hu Old Dominion University Norfolk, Virginia

14th Computational Fluid Dynamics Conference

28 June - 1 July, 1999 / Norfolk, VA

For permission to copy or republish, contact the American Institute of Aeronautics and Astronautics 1801 Alexander Bell Drive, Suite 500, Reston, VA 20191

Application of Discontinuous Galerkin Method to Computational Acoustics

Fang Q. Hu*

Department of Mathematics and Statistics, Old Dominion University, Norfolk, Va 23529

Abstract

An implementation of the discontinuous Galerkin method for the linearized Euler Equations is presented. The emphasis of the paper is on the treatment of boundary conditions and their effectiveness for solving acoustics problems. For far field non-reflecting boundaries, Perfectly Matched Layer (PML) equations are applied and a numerical study on the effectiveness of the PML is carried out. It is found that, when an upwind split flux is used in the discontinuous Galerkin method, the PML equations can offer a numerically stable and effective absorbing boundary condition. In addition, solid wall boundary condition is also discussed. It is shown that not imposing wall boundary condition explicitly will affect the accuracy of the solution.

1 Introduction

Compared to finite difference methods, which has been a favorite choice for many recent studies on computational acoustics^{5,13,15}, the discontinuous Galerkin method has the advantage of being more flexible for complex geometries^{2,3,4,12}. Coupled with its capacity and relative ease of implementation in high order polynomials, it has been recognized as an attractive alternative method for acoustic problems^{2,12}. In this paper, we discuss an implementation of discontinuous Galerkin method for the linearized Euler equations. Emphasis will be given on the treatment of boundary conditions and its effectiveness for solving acoustics problems.

Recently, an analysis on the wave propagation properties of the discontinuous Galerkin method has been carried out¹¹. In that work, the numerical dispersion relation implied in the discontinuous Galerkin method was investigated for a one-dimensional advection equation and a two-dimensional wave equation. It was

found that for a scheme with given order N, there are in general N modes of waves that are supported by the scheme, one physical and the rest non-physical (or numerical parasite modes). Further, the numerical dispersion relation is dependent on the flux formula used in the discretization process. When an upwind type split flux is used, the physical mode can adequately approximate a finite range of low-frequency (long wavelength) waves and is dissipative for high frequency (short wavelength) waves. This is in contrast with the central difference schemes which is non-dissipative for all frequencies and sometimes extra dissipation are introduced to damp the high frequency waves not resolved in the discretization.

In this paper, an implementation of the discontinuous Galerkin method for the linearized Euler equations with a uniform mean flow is presented. In particular, we will investigate the effectiveness of the boundary treatments at solid walls and far field non-reflecting boundaries by the PML technique.

The paper is organized as follows. In section 2, a discretization of the linearized Euler equations is presented. Details on the implementation of numerical boundary conditions are given in section 3. Numerical results are presented in section 4. Section 5 contains the conclusions.

2 Formulation

2.1 Euler equations

The two-dimensional linearized Euler equations in conservation form are written as

$$\frac{\partial \mathbf{u}}{\partial t} + \nabla \cdot \mathbf{F}(\mathbf{u}) = 0 \tag{1}$$

where

^{*}Associate Professor, Senior Member AIAA. Copyright c 1999 by F. Q. Hu. All rights reserved.

$$\mathbf{u} = \begin{bmatrix} \rho \\ u \\ v \\ p \end{bmatrix}, \quad \mathbf{F} = [\mathbf{F}_1, \mathbf{F}_2], \quad \nabla = \left[\frac{\partial}{\partial x}, \frac{\partial}{\partial y}\right] \qquad (2) \qquad \sum_{\ell=0}^{L-1} \frac{d\mathbf{C}_{\ell}^{(i)}}{dt} \int \int_{D^{(i)}} p_{\ell}^{(i)} p_{\ell'}^{(i)} dx dy + \int_{\partial D^{(i)}} (\mathbf{F} \cdot \mathbf{n}) p_{\ell'}^{(i)} ds \quad (6)$$

$$\mathbf{F}_{1} = \begin{bmatrix} M_{x} & 1 & 0 & 0 \\ 0 & M_{x} & 0 & 1 \\ 0 & 0 & M_{x} & 0 \\ 0 & 1 & 0 & M_{x} \end{bmatrix} \mathbf{u} \equiv \mathbf{A}_{1} \mathbf{u}$$
 (3)

$$\mathbf{F}_{2} = \begin{bmatrix} M_{y} & 0 & 1 & 0 \\ 0 & M_{y} & 0 & 0 \\ 0 & 0 & M_{y} & 1 \\ 0 & 0 & 1 & M_{y} \end{bmatrix} \mathbf{u} \equiv \mathbf{A}_{2} \mathbf{u}$$
 (4)

The four elements in the solution vector \mathbf{u} in (??) are the density, velocities and pressure, respectively. M_x and M_y are the mean velocities in the x and y directions, normalized by the speed of sound. Here, for simplicity, the mean velocities will be assumed to be constant.

2.2 Discretization

The discontinuous Galerkin method is a finite element method in which the approximation of u may be discontinuous across the element interfaces. Its application to the Euler and Navier-Stokes equations has been studied extensively in many recent works ([2],[3],[4],[12] and references cited therein). For completeness and convenience of discussion, a brief description of the discretization used in the present study is given below.

Let the computational domain D be partitioned into M sub-domains, or elements, denoted as $D^{(i)}$, i = 0, 1, ..., M - 1. In each element $D^{(i)}$, **u** is approximated by an expansion

$$\mathbf{u}^{(i)}(x,y,t) = \sum_{\ell=0}^{L-1} \mathbf{C}_{\ell}^{(i)}(t) p_{\ell}^{(i)}(x,y)$$
 (5)

in which $\{p_{\ell}^{(i)}(x,y) \mid \ell=0,1,...,L-1\}$ is the set of basis functions for element $D^{(i)}$.

Then expansion (??) is substituted into (??) and it is required that

$$\int \int_{D^{(i)}} \left[\frac{\partial \mathbf{u}^{(i)}}{\partial t} + \nabla \cdot \mathbf{F}(\mathbf{u}^{(i)}) \right] p_{\ell'}^{(i)}(x, y) dx dy = 0$$

for $\ell' = 0, 1, ...L - 1$. Upon applying Green's Theorem, the above can be written as

$$\sum_{\ell=0}^{L-1} \frac{d\mathbf{C}_{\ell}^{(i)}}{dt} \int \int_{D^{(i)}} p_{\ell}^{(i)} p_{\ell'}^{(i)} dx dy + \int_{\partial D^{(i)}} (\mathbf{F} \cdot \mathbf{n}) p_{\ell'}^{(i)} ds$$
 (6)

$$-\int \int_{D^{(i)}} \mathbf{F} \cdot \nabla p_{\ell'}^{(i)} dx dy = 0$$

in which $\partial D^{(i)}$ denotes the boundary of element $D^{(i)}$. This yields a system of ordinary differential equations for the expansion coefficients $C_{\ell}^{(i)}(t)$. We note that no evaluation of the spatial derivatives of F is needed in (??). By inverting the mass matrix in (6), the ODE system can be cast into the form

$$\frac{d\mathbf{C}_{\ell}^{(i)}}{dt} = \mathbf{G}(\mathbf{C}_{\ell}^{(i)}) \tag{7}$$

which will be integrated by a Runge-Kutta time integration scheme⁸.

2.3 Quadrilateral elements and basis **functions**

In this paper, only quadrilateral elements will be considered. We assume each element is mapped into a local coordinates of \bar{x} and \bar{y} in $[-1,1] \times [-1,1]$ by a transformation (see Figure 1 and Appendix)

$$\bar{x} = \bar{x}(x, y), \quad \bar{y} = \bar{y}(x, y). \tag{8}$$

For simplicity, the basis functions will be assumed to be the same for all elements when expressed in the local coordinates, denoted as $\{\bar{p}_{\ell}(\bar{x},\bar{y}) \mid \ell=0,1,...,L-1\}$. Furthermore, the basis functions will be taken to be the Legendre polynomials:

$$\bar{p}_{\ell}(\bar{x},\bar{y}) = P_n(\bar{x})P_m(\bar{y})$$

where P_{α} denotes the Legendre polynomial of order α . The number of polynomials in the basis, L, is related to the order of the scheme, N. For a basis formed by the tensor product of Legendre polynomials up to order $N, L = N^2$. For a basis formed by retaining only those necessary for the completeness of the order, $L=\frac{1}{2}N(N+1)$. As shown in reference [11], wave propagation properties of the scheme improves significantly as the order increases. For this reason, order-complete basis will be used in this paper.

Under the transformation (??), we have

$$dxdy = |J| d\bar{x}d\bar{y}$$

where J is the Jacobian $\frac{\partial(x,y)}{\partial(\bar{x},\bar{y})}$. Due to the orthogonality properties of the Legendre polynomials, the mass matrix in (??) will be a diagonal matrix when transformation (??) is linear and J is constant. When Jacobian J is not constant, the mass matrix will not be, in general, a diagonal matrix. For the transformation given in the Appendix, Jacobian J is constant only if the element is a parallelogram.

In addition, all integrals in (6) will be evaluated numerically using quadrature rules.

2.4 Numerical flux

One of the major difficulties of the discontinuous Galerkin method lies on the evaluation of the flux $\mathbf{F} \cdot \mathbf{n}$ appeared in the middle term in (??). An upwind approach will be used in the present paper. For the linearized Euler equations considered here, we split the \mathbf{F} vector according to the eigenvalues of the matrices \mathbf{A}_1 and \mathbf{A}_2 in (??) and (??). Specifically, we have

$$\mathbf{A}_1 = \mathbf{A}_1^+ + \mathbf{A}_1^- = \begin{bmatrix} M_x & \frac{1}{2}M_x + \frac{1}{2} & 0 & -\frac{1}{2}M_x + \frac{1}{2} \\ 0 & \frac{1}{2}M_x + \frac{1}{2} & 0 & \frac{1}{2}M_x + \frac{1}{2} \\ 0 & 0 & M_x & 0 \\ 0 & \frac{1}{2}M_x + \frac{1}{2} & 0 & \frac{1}{2}M_x + \frac{1}{2} \end{bmatrix}$$

$$+ \begin{bmatrix} 0 & -\frac{1}{2}M_x + \frac{1}{2} & 0 & \frac{1}{2}M_x - \frac{1}{2} \\ 0 & \frac{1}{2}M_x - \frac{1}{2} & 0 & -\frac{1}{2}M_x + \frac{1}{2} \\ 0 & 0 & 0 & 0 \\ 0 & -\frac{1}{2}M_x + \frac{1}{2} & 0 & \frac{1}{2}M_x - \frac{1}{2} \end{bmatrix}$$

and

$$\mathbf{A}_{2} = \mathbf{A}_{2}^{+} + \mathbf{A}_{2}^{-} \equiv \begin{bmatrix} M_{y} & 0 & \frac{1}{2}M_{y} + \frac{1}{2} & -\frac{1}{2}M_{y} + \frac{1}{2} \\ 0 & My & 0 & 0 \\ 0 & 0 & \frac{1}{2}M_{y} + \frac{1}{2} & \frac{1}{2}M_{y} + \frac{1}{2} \\ 0 & 0 & \frac{1}{2}M_{y} + \frac{1}{2} & \frac{1}{2}M_{y} + \frac{1}{2} \end{bmatrix}$$

$$+ \begin{bmatrix} 0 & 0 & -\frac{1}{2}M_y + \frac{1}{2} & \frac{1}{2}M_y - \frac{1}{2} \\ 0 & 0 & 0 & 0 \\ 0 & 0 & \frac{1}{2}M_y - \frac{1}{2} & -\frac{1}{2}M_y + \frac{1}{2} \\ 0 & 0 & -\frac{1}{2}M_y + \frac{1}{2} & \frac{1}{2}M_y - \frac{1}{2} \end{bmatrix}$$

in which \mathbf{A}_1^+ and \mathbf{A}_2^+ have only non-negative eigenvalues and \mathbf{A}_1^- and \mathbf{A}_2^- have only non-positive eigenvalues. Then the \mathbf{F} vector at the boundary of the element is evaluated as

$$\mathbf{F}_1 = \mathbf{A}_1^+ \mathbf{u}^+ + \mathbf{A}_1^- \mathbf{u}^- \tag{9}$$

and

$$\mathbf{F}_2 = \mathbf{A}_2^+ \mathbf{u}^+ + \mathbf{A}_2^- \mathbf{u}^- \tag{10}$$

where \mathbf{u}^+ and \mathbf{u}^- denote the values of \mathbf{u} calculated using the expansion coefficients of the element to the

left/lower and right/upper of the boundary respectively.

Such a discretization is dissipative and has "built-in" dissipation for short wavelength waves¹¹.

3 Boundary Conditions

Boundary treatment is an integral part of computational acoustics. We will describe the implementation of two types of boundary condition, i.e., the solid wall boundary condition and far field non-reflecting boundary condition.

3.1 Solid wall boundary condition

At a solid wall boundary, the normal component of the velocity field becomes zero. This condition is imposed *implicitly* (or weakly) in the discontinuous Galerkin method through the flux calculation along that boundary^{2,3}. Let the normal vector on the solid boundary (outward from the computational domain) be denoted as $\mathbf{n} = (n_1, n_2)$. Then we have

$$u \cdot n_1 + v \cdot n_2 = 0 \tag{11}$$

for the perturbation and

$$M_x \cdot n_1 + M_y \cdot n_2 = 0 \tag{12}$$

for the mean flow, assuming it also satisfies the boundary condition. By (??) and (??), it follows that

$$\mathbf{F} \cdot \mathbf{n} = \begin{bmatrix} 0 \\ p \cdot n_1 \\ p \cdot n_2 \\ 0 \end{bmatrix}$$
 (13)

on a solid wall boundary. The effectiveness of (??) will be studied in the numerical calculations in Section 4.

3.2 Absorbing boundary condition

At the far field of computational domain, the numerical boundary condition must be such that the out-going waves are not reflected. For this purpose, Perfectly Matched Layers (PML) will be applied at those non-reflecting boundaries. PML domains are added to the exterior of the truncated physical domain so that the out-going waves from the interior computational domain are absorbed without significant reflection.

Since the discontinuous Galerkin implementation is not restricted by any particular coordinate system, it is sufficient to consider only the PML equations for the Cartesian coordinates. We will, thus, assume that any interface between the Euler equations and PML equations is perpendicular to either x or y axis. Inside the PML domain, the solution vector **u** is split and the following PML equations are solved 6,9,10 :

$$\frac{\partial \mathbf{u}_1}{\partial t} + \sigma_x \mathbf{u}_1 + \frac{\partial \mathbf{F}_1(\mathbf{u})}{\partial x} = 0 \tag{14}$$

$$\frac{\partial \mathbf{u}_2}{\partial t} + \sigma_y \mathbf{u}_2 + \frac{\partial \mathbf{F}_2(\mathbf{u})}{\partial y} = 0 \tag{15}$$

$$\mathbf{u} = \mathbf{u}_1 + \mathbf{u}_2 \tag{16}$$

In the above, \mathbf{F}_1 and \mathbf{F}_2 are the same as those in (??) and (??). σ_x and σ_y are the absorbing coefficients introduced for the attenuation of waves. Here they are taken to be constant within an element. We note that equations (??)-(??) recover the Euler equation (??) when $\sigma_x = \sigma_y = 0$.

The PML equations (??) - (??) will again be discretized using the discontinuous Galerkin method. Expand \mathbf{u}_1 and \mathbf{u}_2 as

$$\mathbf{u}_{1}(x, y, t) = \sum_{\ell=0}^{L-1} \mathbf{C}_{1\ell}(t) p_{\ell}(x, y)$$
 (17)

$$\mathbf{u}_{2}(x,y,t) = \sum_{\ell=0}^{L-1} \mathbf{C}_{2\ell}(t) p_{\ell}(x,y)$$
 (18)

in each element in the PML domain. By substituting (??) and (??) into (??) and (??), we get

$$\sum_{\ell=0}^{L-1} \left(\frac{d\mathbf{C}_{1\ell}}{dt} + \sigma_x \mathbf{C}_{1\ell} \right) \int \int_{D_{pml}} p_\ell p_{\ell'} dx dy + \int_{\partial D_{pml}} n_1 \mathbf{F}_1 p_{\ell'} ds \text{ Near the cylinder, elements are adjusted to fit the boundary. Figure 3(a) shows the grid used in the calculation in the Euler domain of $[-10, 10] \times [-10, 10]$.

$$-\int \int_{D_{pml}} \mathbf{F}_1 \frac{\partial p_{\ell'}}{\partial x} dx dy = 0$$
(19) Contour plots of pressure at $t = 2, 4$ and 8 are shown in Figure 3(a)-(c). For this calculation, the PML domain of the pmL domain of$$

for $C_{1\ell}$ and

$$\sum_{\ell=0}^{L-1} \left(\frac{d\mathbf{C}_{2\ell}}{dt} + \sigma_y \mathbf{C}_{2\ell} \right) \int \int_{D_{pml}} p_\ell p_{\ell'} dx dy + \int_{\partial D_{pml}} n_2 \mathbf{F}_2 p_{\ell'} ds$$
 wave exits the computational domain. To further assess the reflection error, the calculation is compared with a reference solution found using a larger computational domain. The maximum difference between the numerical solution of Figure 3 and the reference solution for th

for $C_{2\ell}$. Here, D_{pml} denotes an element in the PML domain. Equations (??) and (??) can be readily solved in a manner similar to (6).

The values of σ_x and σ_y are such that σ_y is the same across an interface perpendicular to x and σ_x is the same across any interface perpendicular to y. Since we have $\sigma_x = \sigma_y = 0$ in the interior domain, this will result in $\sigma_y = 0$ for the left and right PML domains and $\sigma_x = 0$ for the upper and lower PML domains, as shown in Figure 2. For the corner PML domains, both σ_x and σ_y are not zero.

We note that PML equations (12)-(14) with split variables have been shown to be only weakly well posed^{1,7,14} and, indeed, numerical instabilities has been observed in their finite difference implementations. The numerical instabilities, however, are weak and could be overcome by introducing damping or filtering in the finite difference schemes^{9,10,14}. As indicated in numerical results in section 4, due to the "builtin" numerical dissipation of the upwind split flux, numerical stability has been observed for (12)-(14).

4 Numerical Results

Three numerical examples will be shown in this section. Unless stated otherwise, all calculations are carried out using square elements with a length of 2 on each side and 5th order polynomials.

In the first example, the reflection of an acoustic pulse by a circular cylinder is simulated. The cylinder has a radius of 2 and is located at x = -4, y = 0. The acoustic pulse is located at x = 4, y = 0. The pulse is defined by these initial values:

$$\rho = p = e^{-(\ln 2)r^2}, \quad u = v = 0$$

where r is the distance to the center of the pulse. Square elements are used through out the computational domain, except the region near the cylinder. culation in the Euler domain of $[-10, 10] \times [-10, 10]$. Contour plots of pressure at t = 2,4 and 8 are shown in Figure 3(a)-(c). For this calculation, the PML domain has a width of two elements and the values of the absorption coefficients are taken to be 5.

The contour plots show very little reflection as the with a reference solution found using a larger computational domain. The maximum difference between the numerical solution of Figure 3 and the reference solution along the vertical line x = 9 is shown in Figure 4. Since the exiting wave has a magnitude larger than 0.1, the reflection error at the interface between the interior and PML domains is about 1%.

In the second example, the propagation of an acoustic pulse in a uniform mean flow is calculated. Here, $M_x = 0.5, M_y = 0$ and the pulse is initially located at (0,0). The pressure contours at t = 0.8and 12 are shown in Figure 5. The Euler domain is $[-10, 10] \times [-6, 6]$ and the PML domain has a width of 2 elements. The calculation has been carried out for a much longer time and no numerical instability has been observed in the PML domains. A comparison with the exact solution is given in Figure 6. Very good agreement is found. The reflection error is shown in Figure 7 for PML domain width being 1, 2 and 3 elements. A larger error is seen when the width is only one element.

In the third example, the reflection of an acoustic pulse by a solid wall is simulated. The solid wall is located at y=0 and the pulse is initially at x=0, y=06. A mean flow of $M_x = 0.5$, $M_y = 0$ is imposed in this example. Figure 8 shows the contour plots of pressure for t = 8 and 12. Again, the reflection error are quite small. However, a comparison with the exact solution reveals the inadequacy of the wall boundary condition. Figure 9 shows the comparisons with the exact solution along a vertical line through the center of the pulse at x = 4 and t = 8. Large differences are seen near the wall at y = 0. Increasing the order of polynomials from 5 to 6 dose not reduce the error. The error, however, decreases when the size of the element is reduced from 2×2 to 1×1 . This is believed to be related to the fact that the solid wall boundary condition, i.e., v = 0, is not imposed explicitly. In fact, v is not zero along the wall. Figure 10 shows the normal velocity v along the wall at y = 0 and t = 8. It is seen that v decreases when smaller elements are used. The magnitude of v is about the same as that of the errors of pressure along the wall.

5 Conclusions

A numerical study on the application of the discontinuous Galerkin method to computational acoustics has been carried out. It is found that Perfectly Matched Layer (PML) equations can offer a numerically stable and effective non-reflecting boundary conditions for the out-going acoustic waves. In addition, since the solid wall condition is not imposed explicitly, it affects the the accuracy of the numerical solution.

References

- [1] S. Abarbanel and D. Gottlieb, A Mathematical Analysis of the PML Method, Journal of Computational Physic, Vol. 134, 357, 1997.
- [2] H. L. Atkins and C. W. Shu, Quadrature-Free Implementation of Discontinuous Galerkin Method for Hyperbolic Equations, AIAA Journal, Vol. 36, 775, 1998.

- [3] F. Basis and S. Rabey, A high-order accurate discontinuous finite element method for the numerical solution of the compressible Navier-Stokes equations, Journal of Computational Physic, Vol. 131, 267, 1997.
- [4] B. Cockburn and C.-W. Shu, The Runge-Kutta discontinuous Galerkin finite-element method for conservative laws, Journal of Computational Physic, Vol. 141, 199, 1998.
- [5] J. C. Hardin, J. R. Ristorcelli and C. K. W. Tam, ICASE/LaRC Workshop on Benchmark Problems in Computational Aeroacoustics (CAA), NASA CP3300, 1995.
- [6] M. E. Hayder, F. Q. Hu, M. Y. Hussaini, Towards Perfectly Absorbing Boundary Conditions for Euler Equations, ICASE Report No. 97-25, to appear in AIAA Journal.
- [7] J. S. Hesthaven, On the Analysis and Construction of Perfectly Matched Layers for the Linearized Euler Equations, Journal of Computational Physic, Vol. 142, 129, 1998.
- [8] F. Q. Hu, M. Y. Hussaini and J. L. Manthey, Lowdissipation and low-dispersion Runge-Kutta schemes for computational acoustics, Journal of Computational Physic, Vol. 124, 177, 1996.
- [9] F. Q. Hu, On Absorbing Boundary Conditions for Linearized Euler Equations by a Perfectly Matched Layer, Journal of Computational Physic, Vol. 129, 201, 1996.
- [10] F. Q. Hu, On Perfectly Matched Layer as an Absorbing Boundary Condition, AIAA paper 96-1664, 1996.
- [11] F. Q. Hu, M. Y. Hussaini and P. Rasetarinera, An Analysis of the Discontinuous Galerkin Method for Wave Propagation Problems, Journal of Computational Physic, Vol. 151, 921, 1999.
- [12] R. B. Lowrie, P. L. Roe and B. Van Leer, A spacetime discontinuous Galerkin method for the timeaccurate numerical simulation of hyperbolic conservative laws, AIAA paper 95-1658, 1995.
- [13] J. S. Shang, High-order compact-difference schemes for time-dependent Maxwell equations, AIAA paper 98-2471, 1998.
- [14] C. K. W. Tam, L. Auriault and F. Cambuli, Perfectly Matched Layer as an Absorbing Boundary Condition for the Linearized Euler Equations in

Open and Ducted Domains, Journal of Computational Physic, Vol. 142, 129, 1998.

[15] C. K. W. Tam and J. C Hardin, Second Computational Aeroacoustics (CAA) Workshop on Benchmark Problems, NASA CP3352, 1997.

Appendix

Mapping of a quadrilateral element

Let $\mathbf{r} = (x, y)$ and the four points of a quadrilateral be denoted as \mathbf{r}_0 , \mathbf{r}_1 , \mathbf{r}_2 and \mathbf{r}_3 . The a mapping to $[-1, 1] \times [-1, 1]$ in (\bar{x}, \bar{y}) can be expressed as

$$\mathbf{r} = \frac{1}{4}(\mathbf{r}_0 + \mathbf{r}_1 + \mathbf{r}_2 + \mathbf{r}_3) + \frac{\bar{x}}{4}(-\mathbf{r}_0 + \mathbf{r}_1 + \mathbf{r}_2 - \mathbf{r}_3)$$

$$+\frac{\bar{y}}{4}(-\mathbf{r}_0-\mathbf{r}_1+\mathbf{r}_2+\mathbf{r}_3)+\frac{\bar{x}\bar{y}}{4}(\mathbf{r}_0-\mathbf{r}_1+\mathbf{r}_2-\mathbf{r}_3)$$

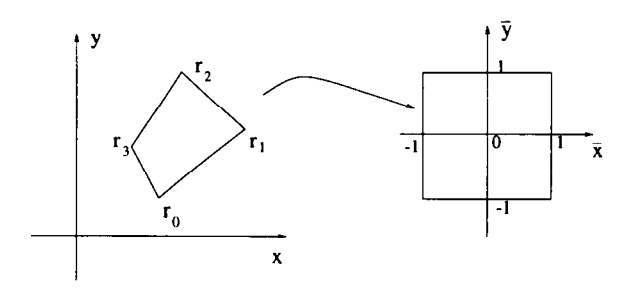


Figure 1. Mapping of a quadrilateral.

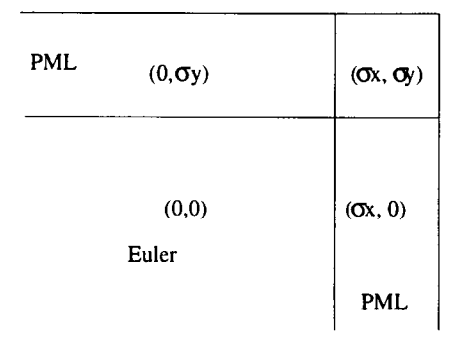
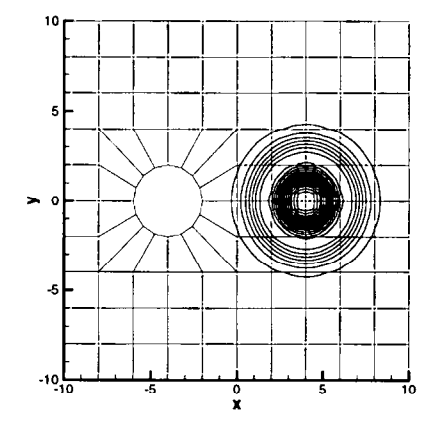
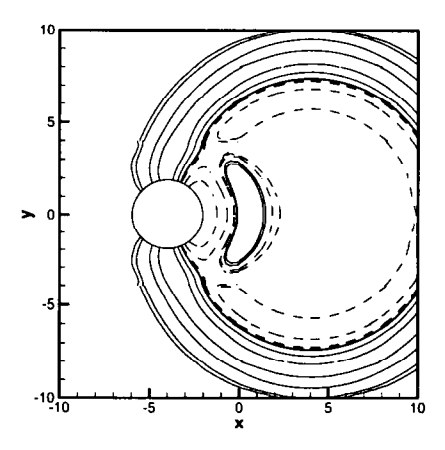


Figure 2. Schematics of PML absorption coefficients.





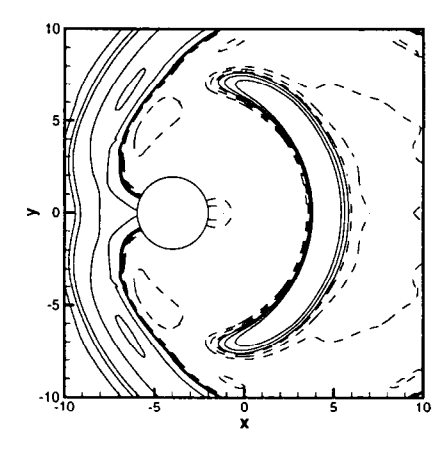


Figure 3. Reflection of an acoustic pulse by a circular cylinder. Shown are the pressure contours and Galerkin elements used. Contour levels at ± 0.1 , ± 0.05 , ± 0.01 , ± 0.005 , ± 0.001 . (a) t = 2, (b) t = 8, (c) t = 12.

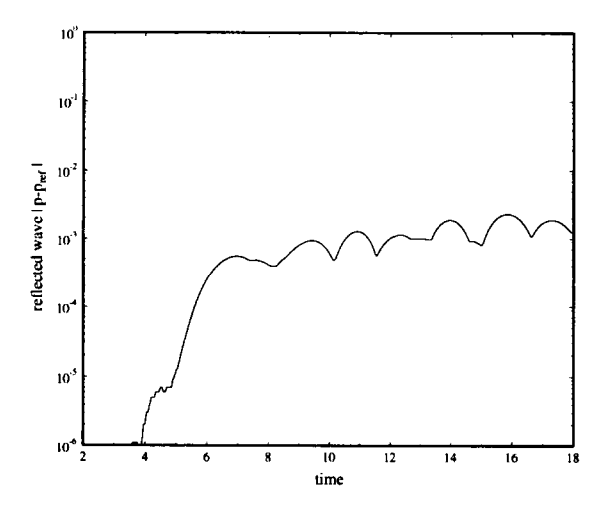
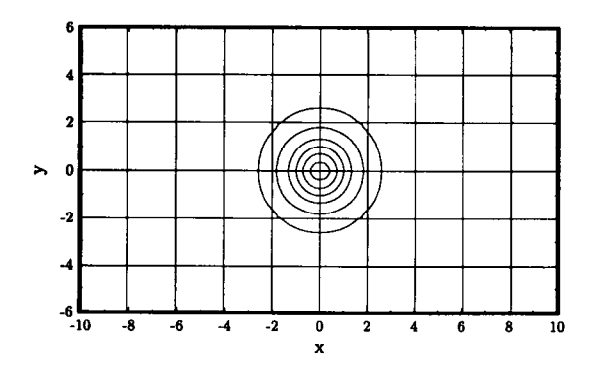
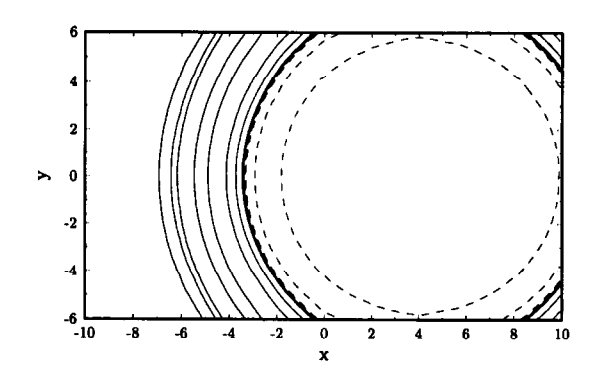


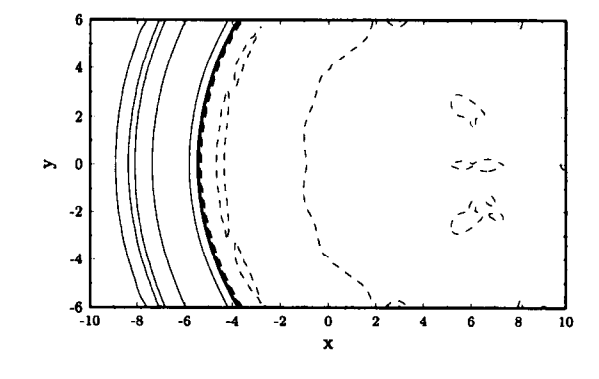
Figure 4. Reflection error, maximum difference between the numerical and reference solutions along x = 9.



$$5(a) t = 0$$



$$5(b) t = 8$$



5(c) t = 12

Figure 5. Propagation of an acoustic pulse in a uniform mean flow $M_x = 0.5$, $M_y = 0$. Shown are the pressure contours at levels ± 0.1 , ± 0.05 , ± 0.01 , ± 0.005 , and ± 0.001 . (a) t = 0, (b) t = 8, (c) t = 12.

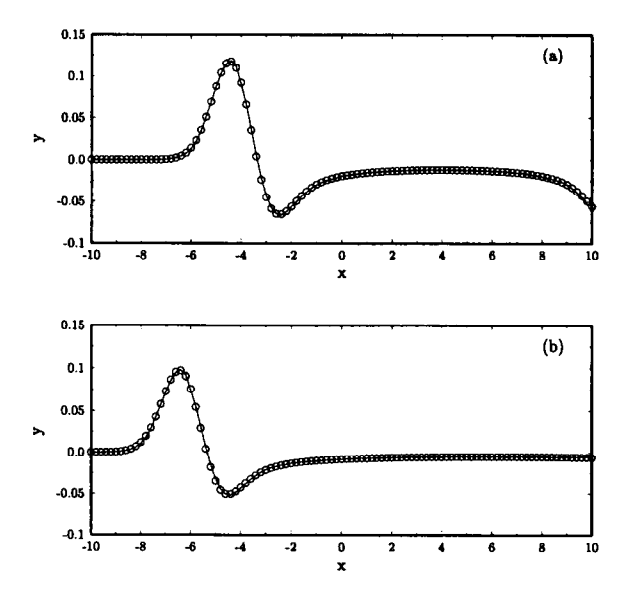


Figure 6. Comparison with exact solution. Solid line: numerical; symbol: exact. (a) t = 8, (b) t = 12.

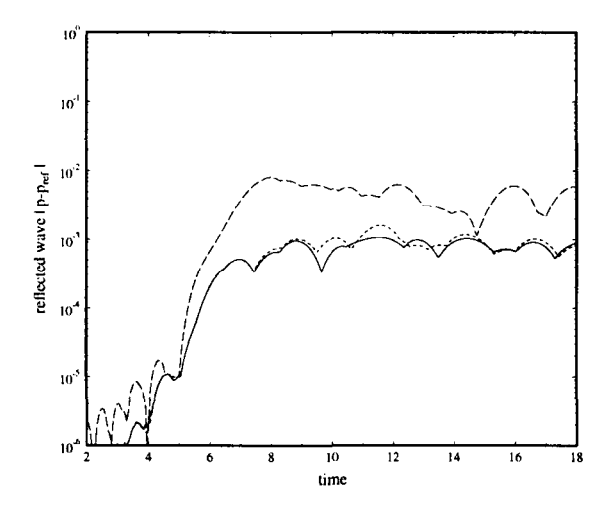
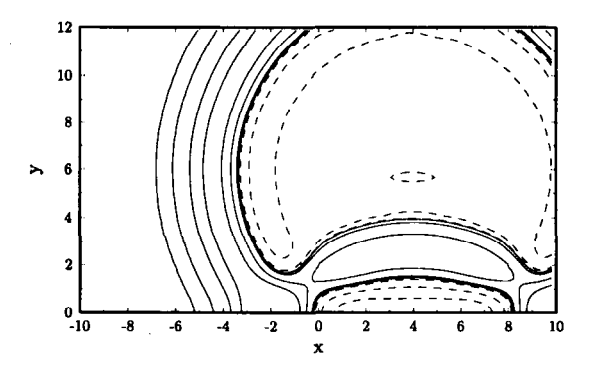
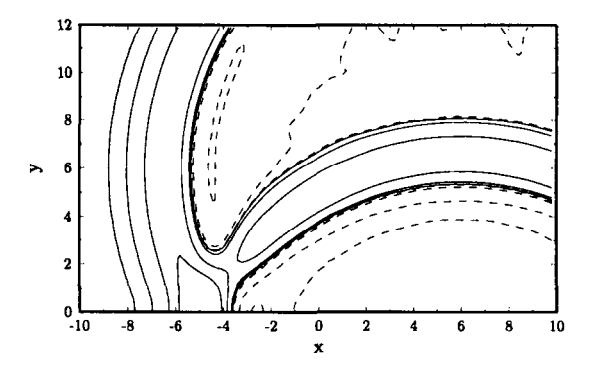


Figure 7. Reflection error, maximum difference between the numerical and reference solutions along x = 9. dashed line: 1 element; dotted line: 2 elements; solid line: 3 elements.



$$8(a) t=8$$



8(b) t=12

Figure 8. Reflection of an acoustic pulse by a solid wall at y=0. $M_x=0.5$, $M_y=0$. Shown are the pressure contours at levels ± 0.1 , ± 0.05 , ± 0.01 , ± 0.005 , and ± 0.001 . (a) t=8, (b) t=12.

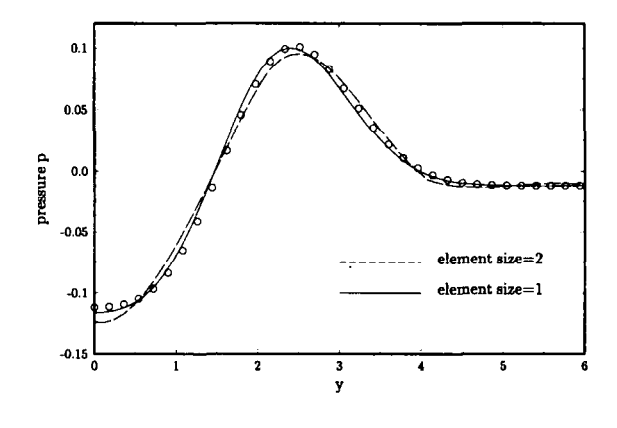


Figure 9. Comparison with exact solution. dashed line: order 5 and 6; solid line: order 5: symbol: exact.

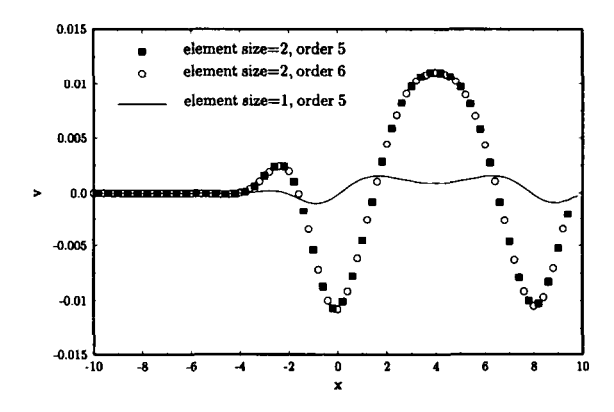


Figure 10. Normal velocity v along the solid wall y = 0 at time t = 8. The size of the elements are 2×2 , symbol, and 1×1 , solid line.